Journal of the Mechanics and Physics of Solids 59 (2011) 1717–1730

Contents lists available at ScienceDirect

Journal of the Mechanics and Physics of Solids

journal homepage: www.elsevier.com/locate/jmps

Size-dependent fracture of Si nanowire battery anodes

Ill Ryu [a,*], Jang Wook Choi [b], Yi Cui [a], William D. Nix [a]

[a] Department of Materials Science and Engineering, Stanford University, Stanford, CA 94305, USA
[b] Graduate School of Energy, Environment, Water and Sustainability (WCU), Korea Advanced Institute of Science and Technology, 373-1 Guseong Dong, Yuseong Gu, Daejeon 305-701, Republic of Korea

ARTICLE INFO

Article history:
Received 23 December 2010
Received in revised form
24 May 2011
Accepted 11 June 2011
Available online 29 June 2011

Keywords:
Lithiation/delithiation
Large deformation
Fracture
Strain energy release rate
Critical size

ABSTRACT

We use a unique transmission electron microscope (TEM) technique to show that Si nanowires (NWs) with diameters in the range of a few hundred nanometers can be fully lithiated and delithiated without fracture, in spite of the large volume changes that occur in this process. By analyzing the stresses associated with lithiation and delithiation we conclude that the process does not occur by the growth of discrete crystalline phases; rather it occurs by amorphization of the Si NWs followed by diffusion of Li into the structure. By accounting for the large deformation associated with this process and by including the effects of pressure gradients on the diffusion of Li, we show that Si NWs with diameters less than about 300 nm could not fracture even if pre-existing cracks were present in the NW. These predictions appear to be in good agreement with the experiment.

Published by Elsevier Ltd.

1. Introduction

Silicon is one of the most promising anode materials for lithium ion batteries because it has a very high theoretical charging capacity ($\sim$4200 mAh/g). Among various electrode structures tested (Obrovac and Krause, 2007; Kim et al., 2008; Magasinski et al., 2010; Song et al., 2010), silicon nanowires are attractive candidates for electrodes because they provide less constraint on the volume changes that occur during lithium insertion (Chan et al., 2007). A major obstacle to using silicon as an electrode is that it experiences a huge volume expansion – by about 400% – during lithiation/delithiation, which can result in fracture of the nanowires.

A number of models have been developed to deal with this problem. Huggins and Nix (2000) made an initial effort to describe fracture associated with decrepitation during battery cycles using the Griffith criterion in a simple one-dimensional model. Recently, Hu et al. (2010) have used the strain energy release rate as a fracture criteria in two-phase $LiFePO_4/FePO_4$ particles. These models both envisioned lithiation/delithiation as occurring by the growth of discrete Li-rich phases.

To take diffusion of lithium into account, a number of papers have focused on the stresses induced by volumetric strain gradients associated with diffusion. Using the analogy between diffusion and heat flow, diffusion-induced stresses can be modeled as thermal stresses (Prussin, 1961). In models of this type, stresses are generated by the constraints on free expansion, since no stresses develop during free thermal or diffusive expansion. Christensen and Newman (2006a,b) developed a rigorous mathematical model for diffusion-induced stresses and used a critical tensile stress as a fracture criterion. Zhang et al. (2007, 2008) performed detailed numerical simulations of stress evolution in ellipsoidal $LiMn_2O_4$

* Corresponding author. Tel.: +1 6507140731; fax: +1 6507254034.
E-mail address: iryu@stanford.edu (I. Ryu).

0022-5096/$ - see front matter Published by Elsevier Ltd.
doi:10.1016/j.jmps.2011.06.003

Nomenclature

C	concentration [#/nm^3]
C_{max}	maximum lithium concentration [#/nm^3]
D	diffusion coefficient [nm^2/s]
e	unit charge per atom [C/#]
E	Young's modulus [GPa]
i	surface current density [C/(nm^2 s)]
I	total ion current [C/s]
J	mass flux of lithium ion [#/(nm^2 s)]
J_b	surface mass flux of lithium ion [#/(nm^2 s)]
l_x^0	initial length in x direction [nm]
l_y^0	initial length in y direction [nm]
l_z^0	initial length in z direction [nm]
l_x	current length in x direction [nm]
l_y	current length in y direction [nm]
l_z	current length in z direction [nm]
L	length of Si NW [nm]
n_{Li^+}	number of lithium ions inserted [#]
r	radial position [nm]
R	radius of Si NW [nm]
T	temperature [°C]
u	radial displacement [nm]
V_{Si}	volume of Si [nm^3]
V_{final}	final volume [nm^3]
$V_{initial}$	initial volume [nm^3]
$V_{current}$	current volume [nm^3]

Greek

α	extent of lithiation [%]
α_T	thermal expansion coefficient [/°C]
β	stress-diffusion coupling parameter [nm^3]
ε_r	radial strain [·]
ε_θ	tangential strain [·]
ε_z	axial strain [·]
ε_t	transformation strain [·]
ε_{th}	thermal strain [·]
ε_{linear}	linear strain [·]
λ_m	mth zero of 1st order Bessel function of the first kind [·]
ν	Poisson's ratio [·]
ρ	density [g/nm^3]
σ_r	radial stress [GPa]
σ_θ	tangential stress [GPa]
σ_z	axial stress [GPa]
σ_h	hydrostatic stress [GPa]
Ω	partial molar volume of lithium [nm^3/#]

particles and included the effect of pressure gradients on the flux of Li. Verbrugge and Cheng (2008) and Deshpande et al. (2010) derived analytical expressions for the stress evolution during Li diffusion for both the sphere and cylinder geometry and used the tensile stress and strain energy as fracture criteria. Moreover, they Cheng and Verbrugge (2008) suggested that surface tension and modulus could play an important role at the nanometer length scale. Haftbaradaran et al. (2011) have considered various fundamental features of highly nonlinear behavior associated with diffusion at high solute concentrations and compared it with atomistic simulation.

A number of authors have used fracture mechanics to model failure associated with electrochemical shock. Aifantis et al. (2007) have used Griffith's criterion to estimate critical crack size at which cracking will stop. To avoid the assumption of pre-existing cracks, Bhandakkar and Gao (2010) developed a clever cohesive zone model for the nucleation of cracks in a thin strip subjected to diffusion-induced stresses and predicted the critical size below which fracture would be avoided. Woodford et al. (2010) have employed the stress intensity factor to study the growth of a pre-existing dominant flaw in a single-particle electrode. Hu et al. (2010) and Zhao et al. (2010) have also utilized the strain energy release rate as a fracture criterion for electrode particles.

In the present study, we explore two types of models in an effort to obtain insight into the fracture of silicon nanowires subjected to lithiation/delithiation. These modeling results are then directly compared with experiments and they reach a good agreement on the size effect on fracture.

As a first approximation and to illustrate the methodology of our approach, we begin by assuming that discrete phase transformations can occur during the charging/discharging processes, as if a Li_xSi compound exists as an equilibrium phase. Due to the misfit strain between different phases, stresses are generated in order to satisfy mechanical compatibility. However, the stresses using the discrete phase model are much too high for silicon nanowires (Si NWs) to support, and are physically unrealistic, even for the smallest NWs (Beaulieu et al., 2001). Moreover, it has been reported that crystalline silicon quickly transforms to an amorphous phase, when lithium ions diffuse into Si NWs (Limthongkul et al., 2003; Chan et al., 2009). Due to the rapid phase transformation, Li_xSi compounds might not exist as equilibrium phases. When the amorphous phase is formed, diffusion might come into play in the stress evolution. If the lithium ion concentration changes gradually in space, the reason for stress evolution is not the amount of inserted lithium, but rather the lithium concentration gradient. By coupling the stresses to the composition gradients, the stress evolution during lithium ion diffusion may be calculated.

Following the work of many others, we make the analogy between heat transfer and diffusion of matter in order to deal with diffusion-driven deformation (Prussin, 1961; Christensen and Newman, 2006a; Verbrugge and Cheng, 2008; Cheng and Verbrugge, 2008; Deshpande et al., 2010; Bhandakkar and Gao, 2010). However, because the volume expansion is huge, the relationship between the fictitious thermal expansion coefficient and partial molar volume needs to be adjusted to be consistent with large deformation. Moreover, the huge volume expansion and associated pressure can affect the

chemical potential, thus affecting the driving force for diffusion. As we will see, this effect can be taken into account by modifying the diffusivity to be a function of the lithium concentration.

Our fracture predictions are made as follows. After computing the stresses associated with a given concentration gradient, we compute the strain energy release rate, using the J-integral method, for sharp cracks of all possible lengths. The J-integral calculation is described in detail in Appendix B. By comparing the maximum possible strain energy release rate with the fracture toughness of Si, we determine whether a NW of that particular size would fail. In this way we estimate the critical size of the Si NWs below which fracture would not occur.

We also performed experiments to determine the critical NW diameter for fracture during the lithiation process. We developed a unique transmission electron microscope (TEM) technique that allows us to observe a single NW before and after the lithiation process. This characterization tool on a single NW scale directly determines a critical diameter for fracture and also serves as a standard to judge the validity of our modeling.

2. Analytical model

2.1. Stresses associated with transformation strains in a cylinder

We begin by writing general relations for the stresses and displacements associated transformation strains in a cylinder. The constitutive law in the cylindrical coordinate system can be expressed by (Zhang et al., 2007)

$$\varepsilon_r-\varepsilon_t(r)=\frac{1}{E}[\sigma_r-\nu(\sigma_\theta+\sigma_z)] \tag{1a}$$

$$\varepsilon_\theta-\varepsilon_t(r)=\frac{1}{E}[\sigma_\theta-\nu(\sigma_r+\sigma_z)] \tag{1b}$$

$$\varepsilon_z-\varepsilon_t(r)=\frac{1}{E}[\sigma_z-\nu(\sigma_r+\sigma_\theta)] \tag{1c}$$

where $\varepsilon_t(r)$ is transformation strain at a particular point, which is related to the partial molar volume (Ω) and concentration, $C(r)$, of lithium ions at that point by

$$\varepsilon_t(r)=\frac{\Omega C(r)}{3} \tag{2}$$

The equilibrium condition and kinematic relations in the cylindrical coordinate system can be expressed by

$$\frac{d\sigma_r}{dr}+\frac{\sigma_r-\sigma_\theta}{r}=0,\quad \varepsilon_r=\frac{du}{dr},\quad \varepsilon_\theta=\frac{du}{r} \tag{3a, b, c}$$

where u is the displacement in the radial direction.

From these relations, u and σ_z can be computed for plane strain conditions as

$$u(r)=\left(\frac{1+\nu}{1-\nu}\right)\left[(1-2\nu)\frac{r}{R^2}\int_0^R \varepsilon_t(r)rdr+\frac{1}{r}\int_0^R \varepsilon_t(r)rdr\right] \tag{4}$$

$$\sigma_z(r)=\frac{E}{1-\nu}\left[\frac{2\nu}{R^2}\int_0^R \varepsilon_t(r)rdr-\varepsilon_t(r)\right] \tag{5}$$

For generalized plane strain conditions, for which the resultant force along the NW is zero, the stresses and displacements in the radial direction are modified as (Timoshenko and Goodier, 1970)

$$\sigma_z(r)=\frac{E}{1-\nu}\left[\frac{2}{R^2}\int_0^R \varepsilon_t(r)rdr-\varepsilon_t(r)\right] \tag{6}$$

$$u(r)=\left(\frac{1-3\nu}{1-\nu}\right)\frac{r}{R^2}\int_0^R \varepsilon_t(r)rdr+\left(\frac{1+\nu}{1-\nu}\right)\frac{1}{r}\int_0^r \varepsilon_t(r)rdr \tag{7}$$

2.2. Discrete phase model

We first consider a discrete phase model wherein a Li_xSi compound is assumed to exist as an equilibrium phase during lithiation/delithiation; this may be modeled using the misfit strain analysis shown in the Fig. 1A. In this model, we follow the same method as the one-dimensional decrepitation model for the bi-layer plate by Huggins and Nix (2000). If the swelling shell were detached from the core, it would expand freely without generating any stresses [Fig. 1B]. Forcing the core-shell structure to remain mechanically compatible during swelling produces residual stresses in both the core and the shell. The shell will be in compression and the core will be in tension [Fig. 1C]. Due to the residual stresses, a mode I crack might grow in the core (Anderson, 2005) during the lithiation process.

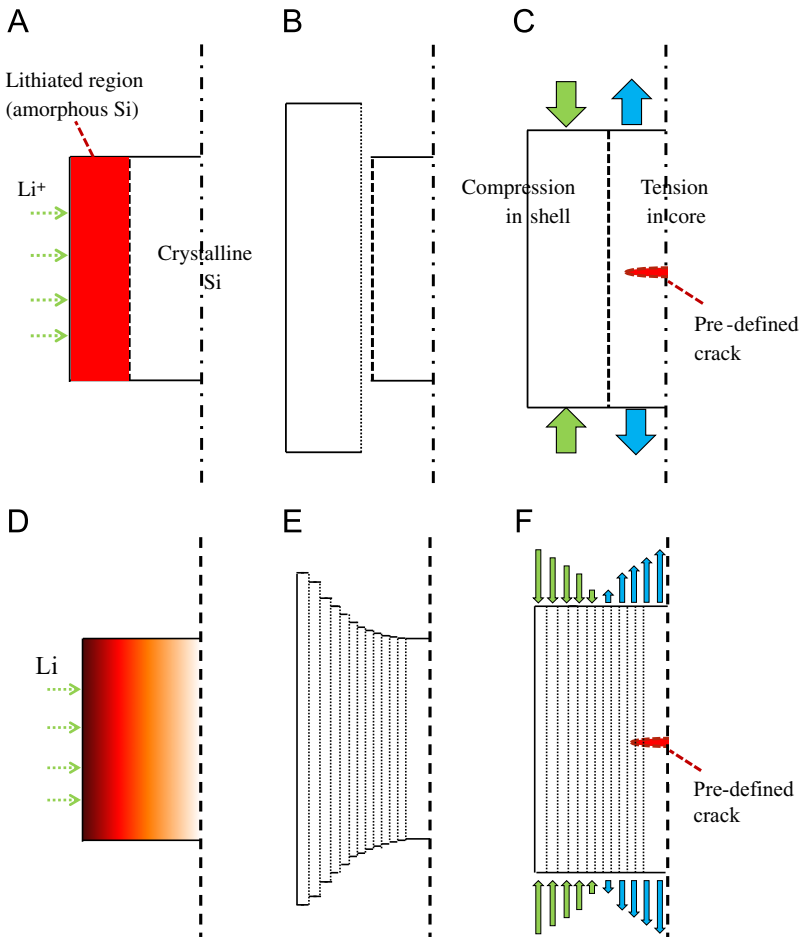

Fig. 1. Model description of discrete phase model (A,B,C) and continuous phase model (D,E,F). (A) Schematic of lithium insertion. (B) Free expansion in the outer shell without the constraint from the core. (C) For mechanically compatible deformation, tension in the core and compression in the shell remain as a residual stress. (D) Schematic of lithium insertion. (E,F) Continuous volume expansion.

Assuming that discrete phases are generated during the lithiation process, the transformed strain is imposed only in the lithiated region, like the misfit strain analysis. Then, the concentration can be expressed with the following equation:

$$C(r)=\begin{bmatrix}0 & (0<r<(1-\alpha)R)\\ C_{max} & ((1-\alpha)R<r<R))\end{bmatrix}=C_{max}\langle r-(1-\alpha)R\rangle^{0} \tag{8}$$

where C_{max} and α are the stoichiometric maximum concentration and extent of lithiation, respectively, and $\langle\cdot\rangle^{0}$ is the Heaviside step function. Combining the concentration (Eq. (8)) with the stress solution (Eq. (6)), the diffusion-induced axial stress is expressed by

$$\sigma_z=\frac{E\Omega C_{max}}{3(1-\nu)}\begin{bmatrix}2\alpha-\alpha^2 (0<r<(1-\alpha)R)\\ 2\alpha-\alpha^2-1 ((1-\alpha)R<r<R)\end{bmatrix} \tag{9}$$

which is shown graphically in the Fig. 2. From this model we can see that the maximum stress resulting from the 400% volume expansion, would be comparable to Young's modulus, which is so high that all Si NWs would fracture, regardless of their diameters. Since NWs of small diameter do not fracture, we conclude that the discrete phase model is completely unrealistic.

2.3. Continuous phase model

If an amorphous phase is generated in the early stages of lithiation, discrete Li-rich phases may not exist. In this sense, we can imagine the existence of a continuous amorphous phase with a continuous concentration distribution, as shown in Fig. 1D–F. As lithium ions flow into the Si NW, the concentration distribution would be continuous, so the transformation

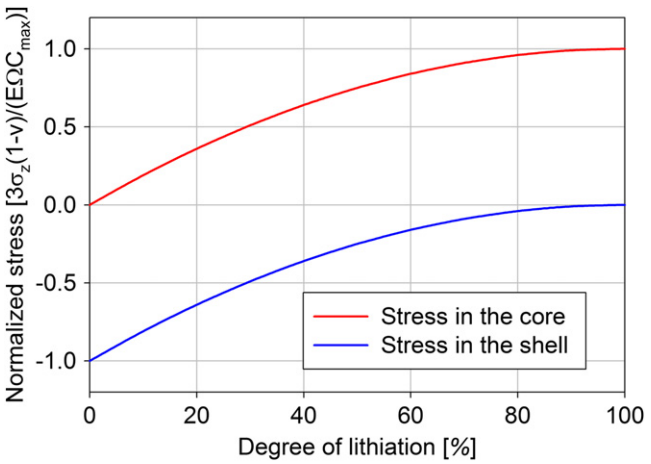

Fig. 2. Normalized diffusion induced stress in z direction with respect to the degree of lithiation.

strain would also vary continuously with position. Like the discrete phase model, the central core of the NW would still be in tension during lithiation and a mode I crack could still grow during lithiation.

To deal with the diffusive flow of lithium, the governing diffusion equation and boundary conditions are expressed by (Deshpande et al., 2010)

$$\frac{\partial C}{\partial t} = D\nabla^2 C = D\left[\frac{\partial^2 C}{\partial^2 r} + \frac{1}{r}\frac{\partial C}{\partial r}\right] \tag{10a}$$

$$\text{at } r=0 \quad -D\left.\frac{\partial C}{\partial r}\right|_{r=0} = 0 \quad \text{(Due to the symmetry)} \tag{10b}$$

$$\text{at } r=R \quad -D\left.\frac{\partial C}{\partial r}\right|_{r=\rho} = -J_b \quad \text{(Constant influx)} \tag{10c}$$

where D is the diffusion coefficient of lithium ions. The analytical solution for this problem is expressed by (Crank, 1980)

$$C(r,t) = \frac{J_b}{2DR}r^2 + \frac{2J_b}{R}t - \frac{RJ_b}{4D} - \frac{2RJ_b}{D}\sum_{m=1}^{\infty}\frac{e^{-D\lambda_m^2 t/R^2}}{\lambda_m^2}\frac{J_0(\lambda_m(r/R))}{J_0(\lambda_m)} \tag{11}$$

where λ_m is the mth zero of the 1st order Bessel function of the first kind.

Combining the stress solution for the case of generalized plane strain (Eq. (6)) with the concentration solution (Eq. (11)), the stress along the axis of the NW can be computed as

$$\sigma_z = \frac{J_b E\Omega R}{12D(1-\nu)} - \frac{J_b E\Omega}{6DR(1-\nu)}r^2 + \frac{2J_b E\Omega R}{3D(1-\nu)}\sum_{m=1}^{\infty}\frac{e^{-D\lambda_m^2 t/R^2}}{\lambda_m^2}\frac{J_0(\lambda_m(r/R))}{J_0(\lambda_m)} \tag{12}$$

Moreover, the displacement in the radial direction is

$$u = \left(\frac{1-3\nu}{1-\nu}\right)\frac{\Omega r}{3R^2}\int_0^R C\cdot r dr + \left(\frac{1+\nu}{1-\nu}\right)\frac{\Omega}{3r}\int_0^r C\cdot r dr \tag{13}$$

Finally, we can compute the radial expansion of the NW as follows:

$$u(R) = \frac{2\Omega J_b}{3}t \tag{14}$$

This can be used to define the external boundary of the problem.

Results for the continuous model are plotted in Fig. 3. From the concentration profiles, we can see that a steady state concentration profile develops after some time ($t > 1000$ s). The stresses associated with these concentration profiles also approach a steady state. These steady states arise because in the present modeling the concentration can rise without limit and is not bounded by the finite solubility of Li in Si. This gives an upper bound on the stresses that can develop during lithiation.

From these analytical models, we have seen that the discrete model cannot be used at all because the stress is much too high under the huge volume expansions that occur. With the continuous phase model, a realistic stress evolution profile can be described. However, there are still several limitations in the analytical model. First of all, amorphization during the lithiation process would lead to changes in material properties as the amorphous phase replaces crystalline Si and the Li_xSi

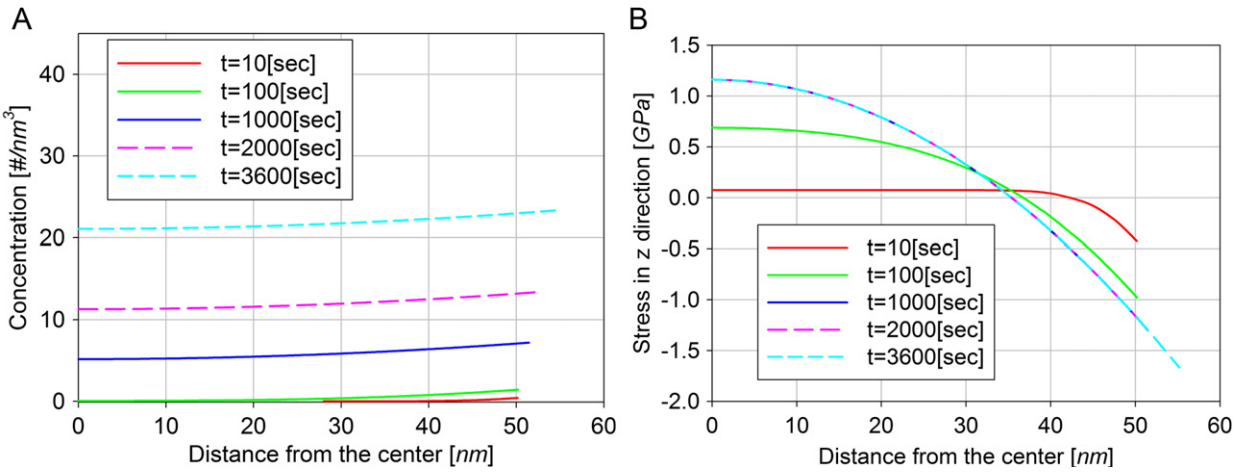

Fig. 3. Diffusion induced stress and concentration in the continuous phase model. (A) Concentration. (B) Stress in z direction.

compounds. Moreover, the maximum stress is not a good measure for fracture resistance, because fracture is expected to be very flaw sensitive. Therefore, it is not possible to judge the tendency for fracture based only on stress. In addition, because the volume expansion is so huge, it is necessary to take a large deformation formulation into account, if we are to utilize the analogy between the thermal expansion and diffusion-induced volume expansion. Finally, the effects of pressure gradients on the flux of Li^+ need to be taken into account, because they can play an important role in relaxing the stress.

3. Numerical model

3.1. Discrete phase model

To calculate the stress field and fracture behavior, a commercial finite element package ABAQUS (2010) (SIMULIA, Providence, RI, USA) is used. As a first approximation, we start with the discrete phase model in which the misfit strain is the driving force for crack growth. In this model, the different material properties of amorphous Si and crystalline Si are used, as shown in Table 1. For intermediate phases, the material properties are calculated using linear interpolation.

In the discrete phase model, the volumetric strain is applied only to the lithiated region, in which the concentration is assumed to be the maximum stoichiometric value.

To evaluate the fracture resistance, we assume that cracks of any size may exist in the wires. We seek the conditions under which none of the assumed pre-existing cracks would grow unstably. When a crack extends under residual stress loading, the strain energy decreases; this is called the strain energy release rate, a measure of the driving force for fracture (Hu et al., 2010; Zhao et al., 2010). To calculate the largest possible strain energy release rate for a NW of a given size, we imagine a pre-existing crack with a length almost equal to the diameter of the core. For different degrees of lithiation, with different core diameters, the strain energy release rate is calculated using a contour integral; the results are plotted in Fig. 4. As lithiation initially progresses by the growth of a thin lithiated shell on the surface of the NW, there is only a small driving force for the relatively large crack to grow. At the other end of the scale, when the Si NW is almost fully lithiated, the length of the crack in the core tends to zero so that the strain energy release rate is also quite small. For these reasons, the strain energy release rate is zero at both ends of the plot, and the maximum strain energy release rate occurs somewhere between the initial state and fully lithiated state, as shown in Fig. 4. Using the fracture toughness of crystalline Si (2 J/m^2) as a criterion for the resistance to fracture (Bhandakkar and Gao, 2010), we find that the discrete phase model makes unrealistic predictions. The strain energy release rates are so high that Si NWs of any size would not support the loading during lithiation based on the misfit stress analysis. Therefore, we expect that lithiation of NWs does not occur by the growth of discrete phases.

3.2. Continuous phase model

As noted above, if an amorphous phase is generated in the early stages of lithiation, discrete Li-rich phases would not exist and a continuous concentration distribution would develop. Again we use the material properties shown in Table 1, and now take the diffusion coefficient of lithium ions in amorphous Si to be 2×10^{-18} m^2/s for the numerical calculations (Bhandakkar and Gao, 2010; Laforge et al., 2008). For comparison with experiments, we use $C/10$ as a charging rate. Because Si is assumed to have theoretical charging capacity of 4200 mAh/g, the charging rate for 10 h is 420 mA/g. The

Table 1
Material properties and operating parameters.

Material	Parameter	Symbol [dimension]	Value	Reference
Crystalline Si	Young's modulus	E [GPa]	185	Wortman and Evans (1965)
	Yield point	σ_y [GPa]	7	Kovacs (1998)
	Poisson's ratio	ν	0.228	Wortman and Evans (1965)
Amorphous Si	Young's modulus	E [GPa]	80	Bhandakkar and Gao (2010)
	Yield point	σ_y [GPa]	1	Sethuraman et al. (2010)
	Poisson's ratio	ν	0.22	Freund and Suresh (2003)
Lithium in Si	Max. concentration	C_{max} [#/nm^3]	53.398	Boukamp et al. (1981)
	Diffusion coefficient	D [nm^2/s]	2	Laforge et al. (2008)
	Partial molar vol.	Ω [nm^3/#]	0.01418	Boukamp et al. (1981)

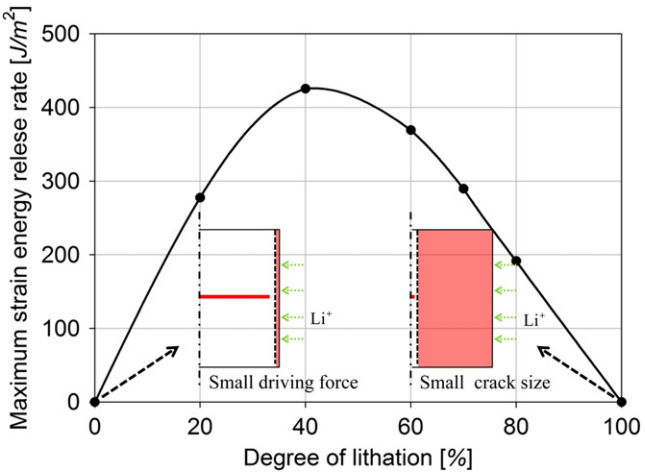

Fig. 4. Maximum strain energy release rate with respect to degree of lithiation in the discrete phase model. Schematic illustrating why strain energy release rate is small at both ends of the scales.

total ion current (I) for the Si NW can be estimated by

$$I = 420\left[\frac{\mathrm{mA}}{\mathrm{g}}\right]\rho\left[\frac{\mathrm{g}}{\mathrm{m}^3}\right]L\pi R^2\left[\mathrm{m}^3\right] = 0.42\rho L\pi R^2\left[\frac{\mathrm{C}}{\mathrm{s}}\right] \tag{15}$$

where ρ is the density of Si, and L and R are the length and radius of the Si NW, respectively. The surface current density (i) is calculated as the total ion current (I) divided by surface area as follows:

$$i = \frac{I}{L2\pi R}\left[\frac{\mathrm{C/s}}{\mathrm{m}^2}\right] = 0.21\rho R\left[\frac{\mathrm{C}}{\mathrm{m}^2\,\mathrm{s}}\right] \tag{16}$$

The surface mass flux (J_b) of Li^+ according to the charging rate is estimated by

$$J_b = \frac{i}{e}\left[\frac{\mathrm{C/m^2\,s}}{\mathrm{C/\#}}\right] = 0.13125\times 10^{19}\rho R\left[\frac{\#}{\mathrm{m}^2\,\mathrm{s}}\right] \tag{17}$$

where e is the unit charge per atom.

As with the discrete phase model, pre-existing cracks of different sizes are assumed to exist and the strain energy release rate is calculated using a contour integral with respect to the diffusive volume expansion. The results of the continuous phase model are plotted in Fig. 5, where the stresses are seen to be several orders or magnitude smaller than for the discrete phase model.

3.3. Analogy for large deformation

Since Si NWs show huge volume expansion during lithiation, the relation between the partial molar volume and fictitious thermal expansion coefficient needs to be modified. The partial molar volume is defined by the volume change

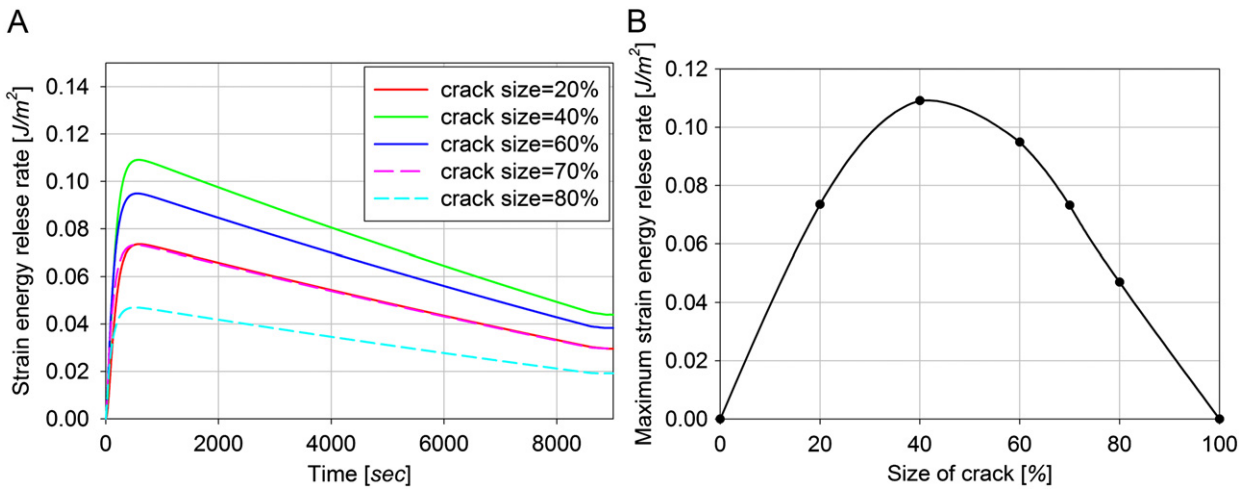

Fig. 5. Strain energy release rate in the continuous phase model. (A) Strain energy release rate with different sizes of pre-defined cracks with respect to time. (B) Maximum strain energy release rate with respect to different sizes of cracks.

with respect to insertion of a lithium ion, and it can be expressed by

$$\Omega \equiv \frac{\partial V}{\partial n_{\mathrm{Li}^+}} \cong \frac{\Delta V}{\Delta n_{\mathrm{Li}^+}}\bigg|_{\text{in } Li_{22}Si_5} = \frac{\Delta V / V_{final}}{\Delta n_{\mathrm{Li}^+} / V_{final}} \tag{18}$$

where n_{Li^+} is number of lithium ions inserted and ΔV is volume change due to the insertion of lithium. Here V_{final} is the volume for the fully lithiated state ($Li_{22}Si_5$). Using the data from Boukamp et al. (1981), the partial molar volume is calculated as follows:

$$\Omega = \frac{3.12}{(22 \times 16/6.592) \times 4.12} = 14.18 \times 10^{-3} \left[\frac{\mathrm{nm}^3}{\#\ \text{of Li}}\right] \tag{19}$$

This value is similar to experimental results (Obrovac et al., 2007), in which the partial molar volume could be assumed a constant during the lithiation. Moreover, the maximum stoichiometric concentration can be computed as follows:

$$C_{max} = \frac{\Delta n_{\mathrm{Li}^+}}{V_{final}} = \frac{16 \times 22}{6.5920} \simeq 53.398 \left[\frac{\#}{\mathrm{nm}^3}\right] \tag{20}$$

where V_{final} is the volume of the fully lithiated phase ($Li_{22}Si_5$). To take advantage of the analogy of thermal expansion and diffusive volume expansion, it has been common practice to use small strain approximations and relate the partial molar volume to the thermal expansion coefficient using the following relation:

$$\alpha_T = \frac{\Omega}{3} \tag{21}$$

The relation between Ω and C_{max} at small strains can then be expressed by

$$\Omega = \frac{\Delta V}{\Delta n_{\mathrm{Li}^+}} = \frac{\Delta V / V_{final}}{\Delta n_{\mathrm{Li}^+} / V_{final}} = \frac{3 \times \varepsilon_{linear}}{C_{max}} \tag{22}$$

The linear strain is about 0.603 for 412% volume expansion. From this linear strain, the partial molar volume is calculated to be

$$\Omega = \frac{3 \times 0.603}{53.398} = 33.87 \times 10^{-3} \left[\frac{\mathrm{nm}^3}{\#}\right] \tag{23}$$

However, the partial molar volume based on the maximum concentration is quite different from the one based on the lattice parameter measurements. We conclude that the above relation based on small deformation may not be used for systems that exhibit such huge volume expansion.

To derive the relation between Ω and C_{max} for large deformation, we started from the definition of the concentration as follows:

$$C = \frac{n_{\mathrm{Li}^+}}{V_{current}} = \frac{n_{\mathrm{Li}^+}}{V_{\mathrm{Si}} + \Omega n_{\mathrm{Li}^+}} \tag{24}$$

where Ω is assumed to be constant.

The transformation dilatation (e_T) is expressed by

$$e_T = \frac{V - V_{Si}}{V_{Si}} = \frac{\Omega n_{Li^+}}{V_{Si}} = \frac{\Omega C}{1 - \Omega C} \tag{25}$$

Now, using the thermal stress analogy, we can obtain

$$\alpha_T = \frac{1}{3}\frac{1}{V}\frac{\partial V}{\partial T} = \frac{1}{3}\frac{\Omega}{(1 - T\Omega)} \tag{26}$$

To determine if this relation holds for small changes in temperature, we take the limit

$$\lim_{T \to 0} \alpha_T(T) = \frac{\Omega}{3} \tag{27}$$

This shows that the relation converges to the result for small deformation. From the finite element calculation, the volume expansion with this thermal expansion coefficient is 412%, which is exactly the same as the reference value.

3.4. Effect of pressure gradient on the flux

In the previous analysis, the flux of lithium ions is expressed by

$$J = -D\nabla C \tag{28}$$

where D is the diffusivity of lithium ions in Si and ∇C is the concentration gradient. However, the flux can be affected by the pressure gradient because the pressure and volume expansion generate a change in the chemical potential gradient. Therefore, the diffusive flux equation needs to be modified to take this effect into account. Adopting the analysis of Zhang et al. (2007) for spherical particles, we re-derive the relation for the cylinder geometry, which is described in Appendix A in detail. As a result, the pressure gradient effect can be dealt with by allowing the diffusivity to be a function of concentration as follows:

$$D = D(C) = D'(1 + \beta C) \tag{29}$$

where D' is constant and β can be expressed by $2\Omega^2 E/9RT(1-\nu)$. We can see the diffusion coefficient increases as the concentration increases. Because a high diffusion coefficient results in a more uniform concentration, the stress is more quickly relaxed when the pressure effects are taken into account.

Based on the modified diffusion coefficient, different crack sizes are pre-defined, and the strain energy release rate is calculated using a contour integral with respect to the diffusive volume expansion, as shown in Fig. 6.

3.5. Critical size for fracture of Si NWs subjected to lithiation/delithiation

Considering all of the above modifications, we now estimate the critical size of Si NWs below, which fracture would not occur. To calculate the critical size, we consider Si NWs of different sizes, and we also change the sizes of the assumed pre-existing cracks to calculate the maximum strain energy release rate, which are plotted in Fig. 7A,B. Through the previous calculation for lithiation [Fig. 6], we found that the maximum strain energy release rate occurs when the radius of the circular crack is about 40% of the radius of the NW. Because it should be independent of NW diameter, we use this size

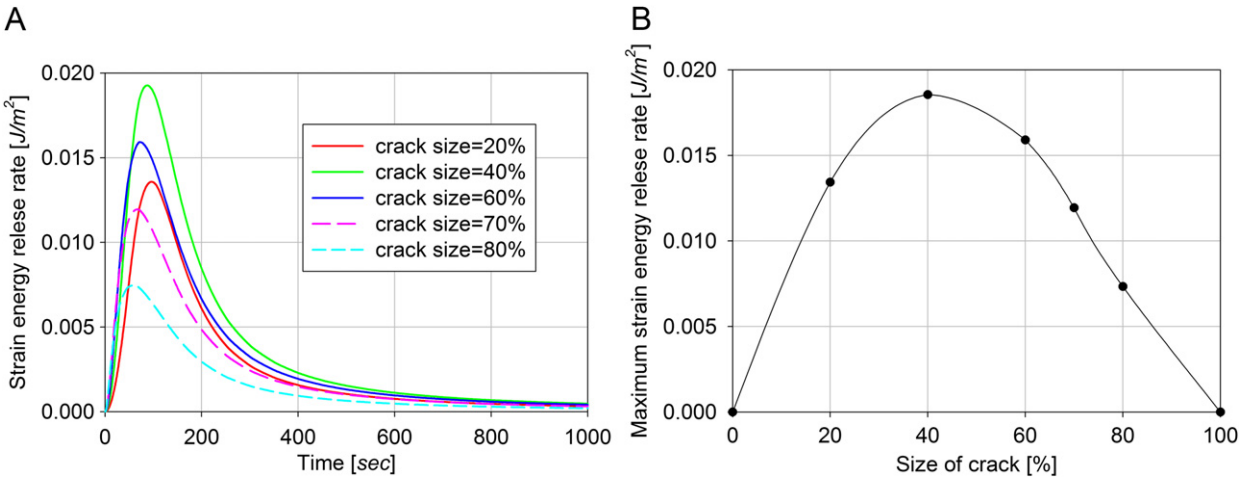

Fig. 6. Strain energy release rate of continuous phase model considering the large deformation formulation and modified diffusivity. (A) Strain energy release rate with different sizes of pre-defined cracks with respect to time. (B) Maximum strain energy release rate with respect to sizes of cracks.

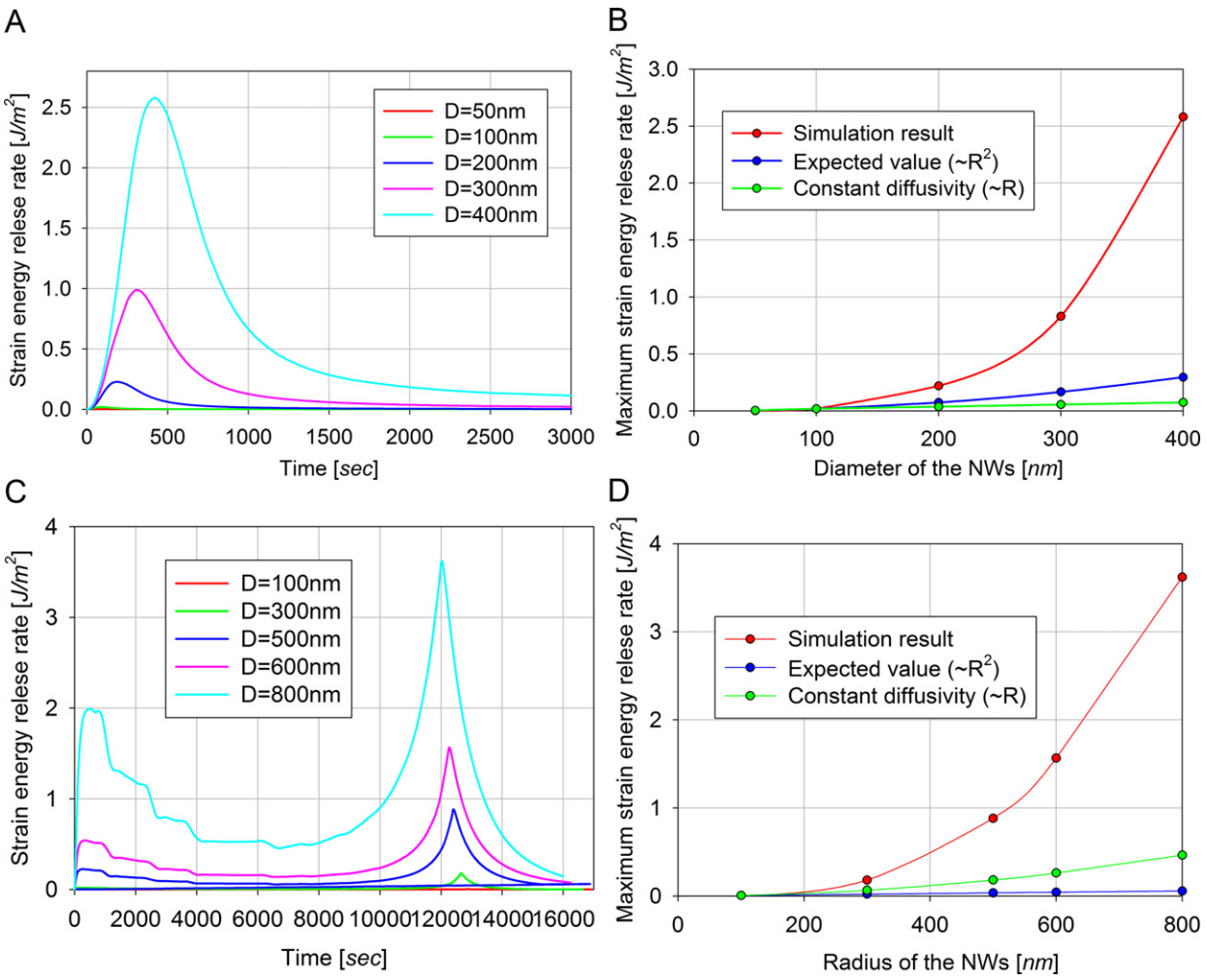

Fig. 7. Strain energy release rate of continuous phase model considering the large deformation formulation and modified diffusivity in different sizes of Si NWs during lithiation(A,B)/delithiation(C,D). (A,C) Strain energy release rates with different Si NW radii with respect to time. (B,D) Maximum strain energy release rate with respect to Si NW radius.

(40%) for the lithiation results in Fig. 7A,B. In the case of delithiation [Fig. 7C,D], we take the depth of the annular crack to be 20% of the NW radius. Because we use the concentration dependent diffusivity and since the flux boundary condition depends on the size of Si NWs, the strain energy release rate might not be a linear or quadratic relation with respect to the size of Si NWs. Indeed, the simulation results demonstrate that the relationship is highly nonlinear. For lithiation, the critical diameter is estimated as 300–400 nm.

For delithiation, the simulation starts with the fully lithiated state in which the lithium ion concentration throughout the nanowire is the stoichiometric maximum concentration. The initial geometry of the fully lithiated state is 400% expanded in volume compared to the initial geometry for lithiation. Since the discharging rate is the same as the charging rate, the flux boundary condition is simply adjusted from in-flux to out-flux with the same magnitude. After the surface concentration reached zero, we changed the boundary condition from constant flux to zero concentration at the surface. As with the case of lithiation, the strain energy release rate is calculated for different sizes of Si NWs in order to estimate the critical size. The results are plotted in Fig. 7C,D. Based on the result, we can see that strain energy release rate increases very quickly, also. For delithiation, the critical crack size is larger than that for lithiation.

4. Experiments

For the experimental study, Si NWs were grown by a VLS process as reported previously (Choi et al., 2010). Si NWs were then dispersed in methanol by sonication. Several drops of the Si NW solution were dropped onto a TEM grid, which had a 20 nm titanium layer deposited on the original TEM carbon layer to ensure good electrical contacts between Si NWs and the TEM grid. The prepared TEM grids went through battery cycling using pouch cells [Fig. 8A]. Detailed experimental

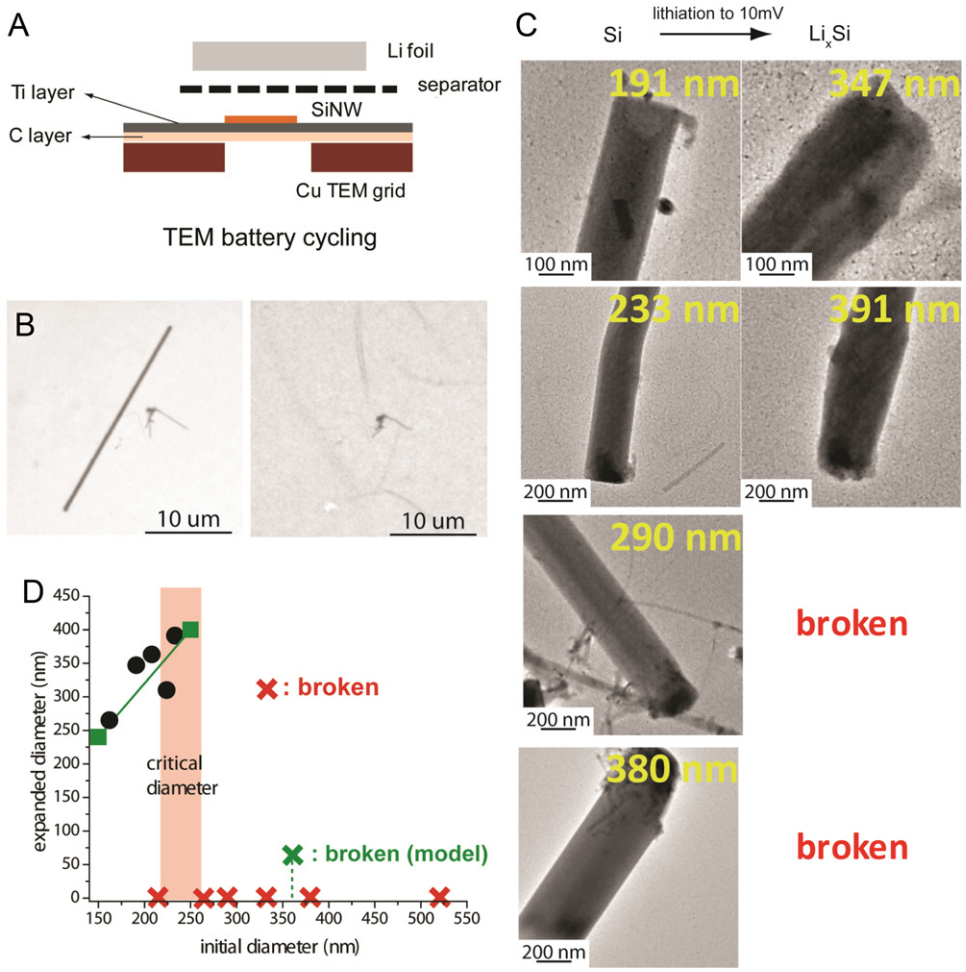

Fig. 8. Mechanical stability testing of a single Si NW during lithiation with ex-situ TEM observation. (A) Schematic illustration of battery cells where Si NWs are loaded on TEM grids. Dimensions of identical Si NWs can be traced during the lithiation processes. (B) TEM images before (left) and after (right) the lithiation process to 10 mV vs. Li/Li^+. These images clearly indicate that large Si NWs disappear due to pulverization during the lithiation process whereas small Si NWs remain in the same position. (C) TEM images of various diameter Si NWs before and after the lithiation processes down to 10 mV. (D) A statistical plot showing critical diameters (220–260 nm) at which Si NWs start pulverizing. Green line shows the model prediction. (For interpretation of the references to color in this figure legend, the reader is referred to the web version of this article.)

procedures for Si NW growth and battery cycling for ex-situ TEM observation are described in Appendix C. Fig. 8B is a typical example of NWs imaged before and after the full lithiation (10 mV vs. Li/Li^+). Hereafter, all potentials described are with regard to the Li redox potential (Li/Li^+). In Fig. 8B, thick NWs ($\sim$500 nm in diameter) located in the middle disappeared after the lithiation, whereas thin NWs ($<$200 nm in diameter) that were located next to the thick ones remained at the same spot. For thick NWs, in most cases NWs disappear after the lithiation. This must be because thick NWs pulverize during the lithiation and are then washed away during the sample washing step with acetonitrile before TEM imaging. Some debris particles are often observed at the spot where thick NWs were originally located. We tested a number of NWs with different diameters for the same lithiation process [Fig. 8C]. From this process we acquired statistics on the critical diameter for NW pulverization [Fig. 8D]. We took $\sim$20 data points in the diameter range of 150–550 nm and from the statistics we conclude that the critical diameter for pulverization is in the regime of 220–260 nm (peach color in Fig. 8D). For this electrochemical process we used a linear scan voltammetry (LSV) technique that scans voltage from open circuit voltage (2.3–2.7 V) to the terminal voltage (10 mV) at a rate of 0.2 mV/s. We also expect that lithiation conditions such as the lithiation rate would change the critical diameter regime because the strain built up along the NW radius depends on the lithiation rate.

5. Discussion

From the results of the misfit strain approach, we can see that the stress evolution associated with discrete phase formation would be too high and unphysical. By comparison, realistic stresses are predicted using the continuous phase

model. Thus, the main driving force for stress generation during lithiation and delithiation appears to be the volumetric strain gradient due to lithium ion diffusion, not the magnitude of the volumetric strain.

Including the effect of the pressure gradient on the diffusional flux of Li greatly increases the rate of diffusion. This also leads to much smaller concentration gradients and smaller stresses compared to the case of diffusion driven by concentration gradients alone. This effect is equivalent to increasing the diffusivity by a factor of around 150.

During lithiation, the strain energy release rate always reaches a maximum in the early stages, after which it decreases [Fig. 7A]. However, the strain energy release rate for delithiation has a local maximum corresponding to early stages and an absolute maximum corresponding to the end of delithiation [Fig. 7C]. These different behaviors can be explained mainly by considering the effect of the pressure gradient. To take the pressure gradient into account we modified the diffusivity to be a linear function of concentration. This causes the behaviors during lithiation (where the lithium content is rising) and delithiation (where the lithium content is declining) to be different. Because a higher lithium concentration and diffusivity lead to faster diffusive flow, the driving force for crack extension during lithiation declines after reaching an early maximum, whereas for delithiation the crack driving force rises after an early maximum. This is why the strain energy release rate is larger during lithiation than during delithiation [Fig. 7A,C].

Because the stresses that develop in the continuous phase model are relatively small, the yield stress in the NW is never exceeded. Even when cracks are assumed to be present, the local stresses remain below the yield stress except near the crack tips. So global yielding effects appear to play an insignificant role in the failure of Si NWs subjected to lithiation/delithiation.

When small deformations are assumed, the maximum strain energy release rates scale linearly with the NW diameter, thus allowing failure of NWs to be described in a non-dimensional way. Since the diffusion coefficient depends linearly on the concentration due to the pressure gradient effect, we may expect that strain energy release rate could be scaled quadratically with the NW diameter. But this kind of non-dimensionalization cannot be used when large deformation and pressure gradient effects are taken into account because the maximum strain energy release rate then depends on the size of the NW in a highly nonlinear way.

Comparing the experimental result, we can see good agreement in the estimation of the critical size of Si NWs for the fracture. There are several reasons why the critical sizes from simulation and experiment are not identical. First of all, it is difficult to replicate the experimental conditions exactly, because the boundary conditions for the experiment are not well known due to the small size of the Si NWs. Secondly, the roughness of the surface, which could make nucleation of cracks easier, was not taken into account in the modeling. Moreover, the material properties for Si during delithiation might be different from those during lithiation. This could explain the observation that Si NWs rarely return to their original shape after battery cycles. Therefore, the critical size for delithiation might be smaller than that for lithiation.

6. Conclusions

By analyzing the stresses associated with lithiation/delithiation of Si NWs and using a fracture mechanics approach to predict fracture, we conclude that NWs with diameters less than about 300 nm would not fail in the lithiation/delithiation process even if pre-existing cracks were present. These predictions are in agreement with in-situ TEM experiments, which show that NWs smaller than a critical diameter, survive this process. By accounting for the large deformation associated with lithiation/delithiation and by including the effects of pressure gradients on the diffusion of Li, we find that Li diffuses rapidly into the NWs, so that only small stresses are created in the process. This helps to explain why the smallest NWs can survive the lithiation/delithiation process even though huge volume changes occur.

Acknowledgment

This work was supported by the Office of Science, Office of Basic Energy Sciences, of the US Department of Energy under contract no. DE-FG02-04ER46163 (IR and WDN). JWC acknowledges the National Research Foundation of Korea Grant funded by the Korean Government (MEST) for the financial support through the Secondary Battery Program (NRF-2010-0029031) and the World Class University Program for the financial support (R-31-2008-000–10055-0). A portion of this work was supported by the Assistant Secretary for Energy Efficiency and Renewable Energy, Office of Vehicle Technologies of the U.S. Department of Energy under contract no. DE-AC02-05CH11231, subcontract no. 6951379 under the Batteries for Advanced Transportation Technologies (BATT). We express our appreciation to Prof. D.M. Barnett, Dr. S.W. Lee,M.T. McDowell of Stanford University and Prof. Y.T. Cheng of the University of Kentucky for helpful discussion about this problem. We also gratefully acknowledge the contributions to this work by Prof. R.A. Huggins of Stanford University, who was the first to recognize this set of problems and who encouraged us and others in this line of work.

Appendix A. Pressure gradient effect on the flux in a cylinder

Using the continuity equation and flux expression, the diffusion equation can be expressed by

$$\frac{\partial c}{\partial t} = -\nabla\cdot\left(-D\left(\nabla c - \frac{c\Omega}{RT}\nabla\sigma_h\right)\right) = D\left(\nabla^2 c - \frac{\Omega}{RT}\nabla c\cdot\nabla\sigma_h - \frac{\Omega c}{RT}\nabla^2\sigma_h\right) \tag{A.1}$$

From the analytical solution for the stress associated with the transformation strains (Timoshenko and Goodier, 1970), the hydrostatic stress can be expressed by

$$\sigma_h(r)=\frac{1}{3}(\sigma_r+\sigma_\theta+\sigma_z)=\frac{E}{3(1-\nu)}\left[\frac{4}{R^2}\int_0^R \varepsilon_T(r)\cdot r dr-2\varepsilon_T(r)\right] \tag{A.2}$$

Now, the gradient of hydrostatic stress may be expressed as

$$\frac{\partial\sigma_h}{\partial r}=\frac{\partial}{\partial r}\left(\frac{E}{3(1-\nu)}\left[\frac{4}{R^2}\int_0^R \varepsilon_T\cdot r dr-2\varepsilon_T\right]\right)=\frac{\partial}{\partial r}\left(\frac{\Omega E}{9(1-\nu)}\left[\frac{4}{R^2}\int_0^R c\cdot r dr-2c\right]\right)=-\frac{2\Omega E}{9(1-\nu)}\frac{\partial c}{\partial r} \tag{A.3}$$

Substituting this expression into the diffusion equation, Eq. (A.1), we get

$$\frac{\partial c}{\partial t}=D\left(\frac{\partial^2 c}{\partial r^2}+\frac{1}{r}\frac{\partial c}{\partial r}+\frac{2\Omega^2 E}{9RT(1-\nu)}\left(\frac{\partial c}{\partial r}\right)^2+\frac{2\Omega^2 Ec}{9RT(1-\nu)}\left(\frac{\partial^2 c}{\partial r^2}+\frac{1}{r}\frac{\partial c}{\partial r}\right)\right) \tag{A.4}$$

If we take diffusivity to be a function of concentration

$$D=D(c)=\tilde{D}(1+\beta c) \tag{A.5}$$

where $\tilde{D}$ and α are assumed to be constant.

Then, using the flux equation and continuity equation, the diffusion equation becomes

$$\frac{\partial c}{\partial t}=-\nabla\cdot J=-\nabla\cdot(\tilde{D}(1+\beta c)\nabla c)=\tilde{D}\left(\frac{\partial^2 c}{\partial r^2}+\frac{1}{r}\frac{\partial c}{\partial r}+\beta\left(\frac{\partial c}{\partial r}\right)^2+\beta c\left(\frac{\partial^2 c}{\partial r^2}+\frac{1}{r}\frac{\partial c}{\partial r}\right)\right) \tag{A.6}$$

which shows that the diffusion equation now involves a concentration dependent diffusivity. Comparing this with the previous expression, we can get an expression for β:

$$\beta=\frac{2\Omega^2 E}{9RT(1-\nu)} \tag{A.7}$$

Interestingly, this relation is same as that for the spherical particle (Zhang et al., 2007).

For Si NWs

$$\beta=\frac{2\Omega^2 E}{9k_B T(1-\nu)}=\frac{2\times(14.18\times10^{-30})^2\times185\times10^9}{9\times(1.38\times10^{-23})\times300\times(1-0.28)}=2.77318\ \ [\mathrm{nm}^3] \tag{A.8}$$

Appendix B. Evaluation of strain energy release rate

In this study, we calculate the contour integral (J-integral) numerically using ABAQUS as a fracture measure. To evaluate these integrals numerically, we intentionally make a rings elements surrounding the crack tip. Based on the stress field near the crack tip, ABAQUS numerically evaluated the J-integral along pre-defined paths near the crack tip. Since the J-integral is path independent, we chose five different paths near the crack tip and confirmed that these values along different paths were converged well. For accuracy, meshes near the crack tip were very dense, with the smallest element around the tip being 10^{-3} times the crack length.

Appendix C. Additional explanation about the experiment

Si NW growth: For the Si NW growth, stainless steel substrates (McMaster-Carr, foil 304) with 50 nm gold layers deposited on top were situated inside a quartz tube (1 in. diameter) in a tube furnace. First, the substrates underwent a pre-growth step at 485 °C for 30 min to break the gold film into nanoparticles. In the subsequent growth step, 2% silane (SiH_4) gas in argon was flown through the tube at 485 °C for about 30 min at a rate of 50 sccm and constant pressure of 40 Torr.

Battery cycling for Si NWs on TEM grids: For the ex-situ TEM process, TEM grids with reference marks (Ted Pella) were used. Titanium layers (~20 nm) were deposited by e-beam evaporation onto original carbon films on the grids to ensure good electrical contacts with Si NWs. VLS grown Si NWs were dissolved in methanol by sonication and several drops of Si NW solution were dropped onto the TEM grids to form TEM grid-based anodes. For battery cycling, pouch cells were made. TEM grid-based anodes were located on copper current collectors and then separators (Asahi Kasei) soaked with electrolyte (1 M $LiPF_6$ in ethylene carbonate/diethyl carbonate (EC/DEC, 1:1 v/v, Ferro Corporation)) and Li foils (Alfa Aesar) were placed on top sequentially (Fig. 8A). After cycling, TEM grid-based anodes were rinsed with acetonitrile thoroughly and then delivered to TEM in sealed vials. TEM grids were loaded into the TEM chamber within 15 s to minimize the period in which the grids were exposed to air.

References

ABAQUS, ver. 6.9-3, 2010. Dassault Systemes Simulia Corp., Providence, RI, USA.

Aifantis, K.E., Hackney, S.A., Dempsey, J.P., 2007. Design criteria for nanostructured Li-ion batteries. J. Power Sources 165, 874–879.

Anderson, T.L., 2005. In: Fracture Mechanics: Fundamentals and Applications third ed. Taylor & Francis.

Beaulieu, L.Y., Eberman, K.W., Turner, R.L., Krause, L.J., Dahn, J.R., 2001. Colossal reversible volume changes in lithium alloys. Electrochem. Solid-State Lett. 4, A137–A140.

Bhandakkar, T.K., Gao, H., 2010. Cohesive modeling of crack nucleation under diffusion induced stresses in a thin strip: Implications on the critical size for flaw tolerant battery electrodes. Int. J. Solids Struct. 47, 1424–1434.

Boukamp, B.A., Lesh, G.C., Huggins, R.A., 1981. All-solid lithium electrodes with mixed-conductor matrix. J. Electrochem. Soc. 128, 725–729.

Chan, C.K., Peng, H., Liu, G., McIlwrath, K., Zhang, X.F., Huggins, R.A., Cui, Y., 2007. High-performance lithium battery anodes using silicon nanowires. Nat. Nanotechnol. 3, 31–35.

Chan, C.K., Ruffo, R., Hong, S.S., Huggins, R.A., Cui, Y., 2009. Structural and electrochemical study of the reaction of lithium with silicon nanowires. J. Power Sources 189, 34–39.

Cheng, Y.-T., Verbrugge, M.W., 2008. The influence of surface mechanics on diffusion induced stresses within spherical nanoparticles. J. Appl. Phys. 104, 083521.

Choi, J.W., McDonough, J., Jeong, S., Yoo, J.S., Chan, C.K., Cui, Y., 2010. Stepwise nanopore evolution in one-dimensional nanostructures. Nano Lett. 10, 1409–1413.

Christensen, J., Newman, J., 2006a. A mathematical model of stress generation and fracture in lithium manganese oxide. J. Electrochem. Soc. 153, A1019–A1030.

Christensen, J., Newman, J., 2006b. Stress generation and fracture in lithium insertion materials. J. Solid State Electrochem. 10, 293–319.

Crank, J., 1980. In: The Mathematics of Diffusion second ed. Oxford University Press, New York.

Deshpande, R., Cheng, Y.-T., Verbrugge, M.W., 2010. Modeling diffusion-induced stress in nanowire electrode structures. J. Power Sources 195, 5081–5088.

Freund, L.B., Suresh, S., 2003. In: Thin Film Materials. Cambridge University Press, New York.

Haftbaradaran, H., Song, J., Curtin, W.A., Gao, H., 2011. Continuum and atomistic models of strongly coupled diffusion, stress, and solute concentration. J. Power Sources 196, 361–370.

Hu, Y., Zhao, X., Suo, Z., 2010. Averting cracks caused by insertion reaction in lithium-ion batteries. J. Mater. Res. 25, 1007–1010.

Huggins, R.A., Nix, W.D., 2000. Decrepitation model for capacity loss during cycling of alloys in rechargeable electrochemical systems. Ionics 6, 57–63.

Kim, H., Han, B., Choo, J., Cho, J., 2008. Three-dimensional porous silicon particles for use in high-performance lithium secondary batteries. Angew. Chem. Int. Ed. 47, 10151–10154.

Kovacs, Gregory T.A., 1998. In: Micromachined Transducers Sourcebook. McGraw-Hill, Inc., New York.

Laforge, B., Levan-Jodin, L., Salot, R., Billard, A., 2008. Study of germanium as electrode in thin-film battery. J. Electrochem. Soc. 155, A181–A188.

Limthongkul, P., Jang, Y.I., Dudney, N.J., Chiang, Y.-M., 2003. Electrochemically-driven solid-state amorphization in lithium–metal anodes. J. Power Sources 119–121, 604–609.

Magasinski, A., Dixon, P., Hertzberg, B., Kvit, A., Ayala, J., Yushin, G., 2010. High-performance lithium-ion anodes using a hierarchical bottom-up approach. Nat. Mater. 9, 353–358.

Obrovac, M.N., Christensen, L., Le, D.B., Dahn, J.R., 2007. Alloy design for lithium-ion battery anodes. J. Electrochem. Soc. 154, A849–A855.

Obrovac, M.N., Krause, L.J., 2007. Reversible cycling of crystalline silicon powder. J. Electrochem. Soc. 154, A103–A108.

Prussin, S., 1961. Generation and distribution of dislocations by solute diffusion. J. Appl. Phys. 32, 1876–1881.

Sethuraman, V.A., Chon, M.J., Shimshak, M., Srinivasan, V., Guduru, P.R., 2010. In situ measurements of stress evolution in silicon thin films during electrochemical lithiation and delithiation. J. Power Sources 195, 5062–5066.

Song, T., Xia, J.L., Lee, J.H., Lee, D.H., Kwon, M.S., Choi, J.M., Wu, J., Doo, S.K., Chang, H., Park, I.W., Zang, D.S., Kim, H., Huang, Y.G., Hwang, K.C., Rogers, J.A., Paik, U., 2010. Arrays of sealed silicon nanotubes as anodes for lithium ion batteries. Nano Lett. 10, 1710–1716.

Timoshenko, S.P., Goodier, J.N., 1970. Theory of Elasticity, third ed. McGraw-Hill, NewYork.

Verbrugge, M.W., Cheng, Y.-T., 2008. Stress distribution within spherical particles undergoing electrochemical insertion and extraction. ECS Trans. 16, 127–139.

Woodford, W.H., Chiang, Y.M., Carter, W.C., 2010. "Electrochemical Shock" of intercalation electrodes: a fracture mechanics analysis. J. Electrochem. Soc. 157, A1052–1059.

Wortman, J.J., Evans, R.A., 1965. Young's modulus, shear modulus, and Poisson's ratio in Silicon and Germanium. J. Appl. Phys. 36, 153–156.

Zhao, K., Pharr, M., Vlassk, J.J., Suo, Z., 2010. Fracture of electrodes in lithium-ion batteries caused by fast charging. J. Appl. Phys. 108, 073517.

Zhang, X., Shyy, W., Sastry, A.M., 2007. Numerical simulation of intercalation-induced stress in Li-ion battery electrode particles. J. Electrochem. Soc. 154, A910–A916.

Zhang, X., Sastry, A.M., Shyy, W., 2008. Intercalation-induced stress and heat generation within single lithium-ion battery cathode particles. J. Electrochem. Soc. 155, A542–552.